Environmental Science & Technology Letters

Letter

pubs.acs.org/journal/estlcu

Effect of Pattern Shape on the Initial Deposition of Particles in the Aqueous Phase on Patterned Membranes during Crossflow Filtration

Dong-Chan Choi,[†] Seon-Yeop Jung,[†] Young-June Won,[‡] Jun H. Jang,[†] Jae-Woo Lee,[†] Hee-Ro Chae,[†] Joowan Lim,[⊥] Kyung Hyun Ahn,[†] Sangho Lee,[§] Jae-Hyuk Kim,[∥] Pyung-Kyu Park,*[,⊥] and Chung-Hak Lee*[,†]

[†]School of Chemical and Biological Engineering, Seoul National University, Seoul 08826, Republic of Korea

[‡]Center for Environment, Health and Welfare Research, Korea Institute of Science and Technology, Seoul 02792, Republic of Korea

[§]School of Civil and Environmental Engineering, Kookmin University, Seoul 02707, Republic of Korea

[∥]Department of Environmental Engineering, Pusan National University, Pusan 46241, Republic of Korea

[⊥]Department of Environmental Engineering, Yonsei University, Wonju, Gangwon-do 26439, Republic of Korea

Supporting Information

ABSTRACT: Patterned membranes for water treatment processes have been proposed to mitigate the detrimental effect of membrane fouling. Analysis of the effects of various pattern shapes on antifouling properties is required to achieve a higher resistance to fouling in these membranes. In this study, membranes for water treatment with unpatterned, pyramid, reverse-pyramid, and 45°-rotated pyramid patterns were prepared, and their antifouling effects were compared by measuring the extent of particle deposition during crossflow filtration. The 45°-rotated pyramid patterns were the most effective in reducing particle deposition. Computational fluid dynamics modeling was conducted for each membrane surface to elucidate the differences between the antifouling properties of various patterns in terms of shear stress and flow regime.

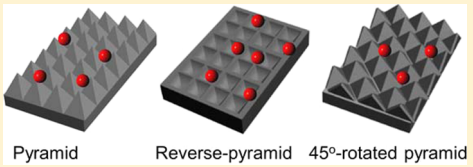

INTRODUCTION

Water purification by membrane filtration is one of the most efficient technologies for alleviating the global shortage of clean water. However, membrane fouling is a major drawback, causing water flux decline and greater requirements for cleaning and replacement.[1−4]

Patterned membranes have been suggested for reducing membrane fouling generally in crossflow operation, which is still widely used in industrial membrane filtration applications. Hollow fiber patterned membranes for water treatment were fabricated, and their antifouling properties were investigated.[5−9] However, the type of pattern under study was limited to "line and void" because a continuous fabrication process with a patterned nozzle was utilized in these previous studies. Membranes with pyramid and/or prism patterns were prepared by combining soft lithography and phase separation methods, which are suitable for patterning discretized shapes.[10,11] However, the investigation of more varied pattern shapes is required to further enhance the antifouling property of patterned membranes.

In this study, membranes with pyramid, reverse-pyramid (R-pyramid), and 45°-rotated pyramid (45-pyramid) patterns were fabricated using soft lithography and non-solvent-induced phase separation (NIPS) methods. An unpatterned membrane was also prepared as a control. To analyze the differences in the effect of pattern shape on the initial deposition of particulate matter, filtration experiments were performed using model particles in crossflow operation mode. The initial particle deposition behavior on the various membranes was analyzed using three-dimensional computational fluid dynamics (CFD).

MATERIALS AND METHODS

Preparation of Membranes. Pyramid, R-pyramid, and 45-pyramid patterned membranes were prepared on patterned polydimethylsiloxane (PDMS) molds using a polyvinylidene fluoride (PVDF) solution. An unpatterned membrane was fabricated with an unpatterned mold. The schematic diagram of the PVDF membrane fabrication procedure is provided as Figure S1. The specifications of materials are also given in the Supporting Information. Further details of the fabrication procedure were published previously.[10] The prepared membranes were characterized using a scanning electron microscope (SEM, JSM-6701F, Jeol USA, Inc.).

Pure Water Flux Measurement. The pure water flux of each unpatterned and patterned membrane was measured using a crossflow filtration system with deionized (DI) water as depicted in Figure S2. A prepared membrane sheet was mounted in a lab-scale membrane module. The effective membrane area was 4 cm^2 with a 2 cm length and a 2 cm width. The channel height of the module was 2 mm. After

Received: December 14, 2016
Revised: January 3, 2017
Accepted: January 5, 2017
Published: January 5, 2017

DOI: 10.1021/acs.estlett.6b00468
Environ. Sci. Technol. Lett. XXXX, XXX, XXX−XXX

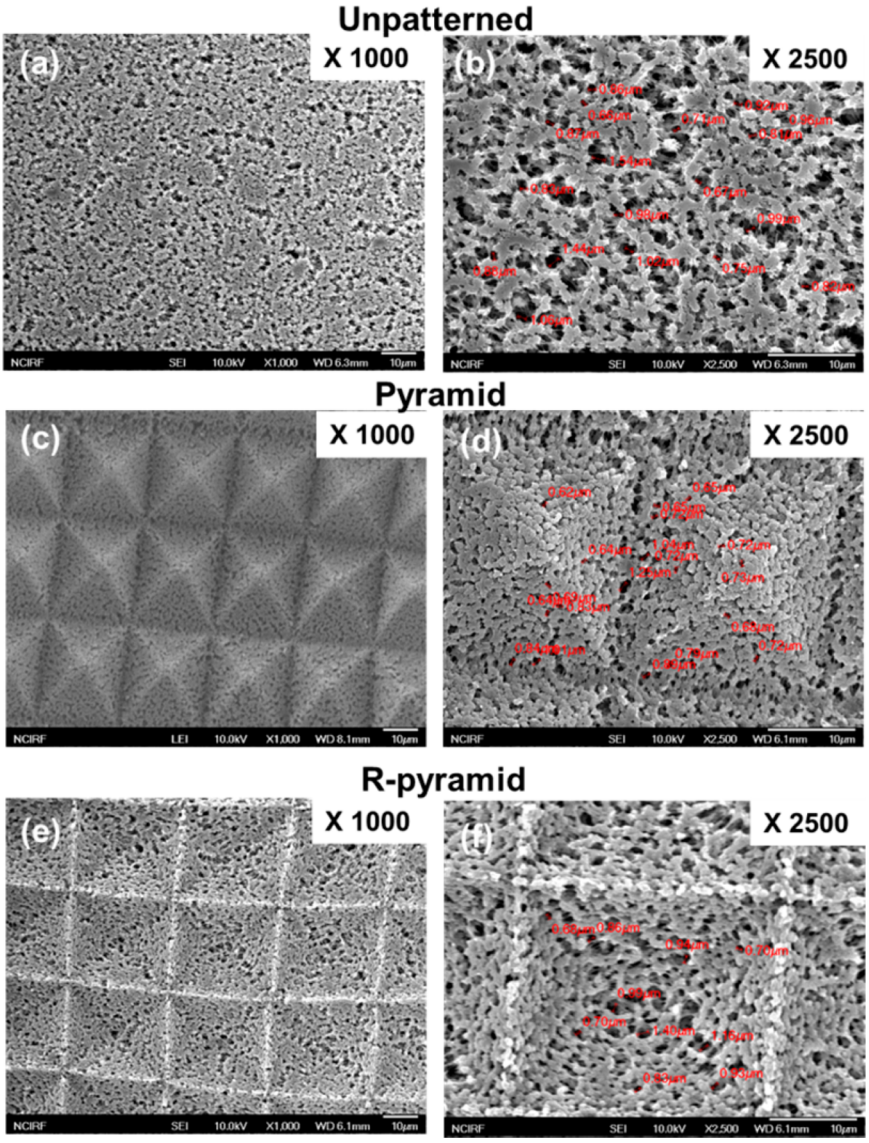

Figure 1. SEM images of prepared PVDF membranes: (a and b) unpatterned, (c and d) pyramid, and (e and f) reverse-pyramid (R-pyramid) patterned membranes.

preoperation of the membrane at 50 kPa for 2 h to attain steady-state water flux, the water flux value was measured at 5, 10, and 15 kPa.

Particle Deposition Experiment. The effects of each pattern on particle deposition were investigated using the same cross filtration system using 1.1 μm polystyrene latex beads. Further details are given in the Supporting Information.

CFD Modeling. The boundary conditions and governing equations for three-dimensional CFD modeling were set as detailed in a previous study.[12] More information is given in the Supporting Information.

RESULTS AND DISCUSSION

Characterization of Membranes. The SEM images of the membranes are shown in Figure 1. Each membrane exhibited submicrometer pores with an average pore size of around 0.9 μm, and the pyramid and R-pyramid patterns were transferred with high fidelity. The pattern shape of the 45-pyramid membrane was almost identical to that of the pyramid membrane except for the orientation of the pattern features (image not shown here). The apparent pure water flux, calculated from the apparent surface area based on geometric cross section, for pyramid, R-pyramid, and 45-pyramid membranes was higher than that of the unpatterned membrane (Figure 2). This enhancement is understood considering that the effective surface area of patterned membranes having the same dimensions as that of the patterned mold is approximately 1.6 times larger than that of an unpatterned membrane, because of the pattern corrugation (Figure S3).[10] The real increase in water flux by patterns was <1.6 because the pattern fidelity of prepared patterned membranes was not exactly unity.

Particle Deposition on Unpatterned and Patterned Membranes. Particle deposition on unpatterned and patterned surfaces is shown in Figure 3. The results show that the level of particle deposition decreased for the three patterned membranes compared with that of the unpatterned membrane and that the particle deposition on the three patterned surfaces differed quantitatively. The 45-pyramid patterned membrane was the most efficient in reducing the level of particle deposition, followed by the pyramid pattern,

DOI: 10.1021/acs.estlett.6b00468
Environ. Sci. Technol. Lett. XXXX, XXX, XXX−XXX

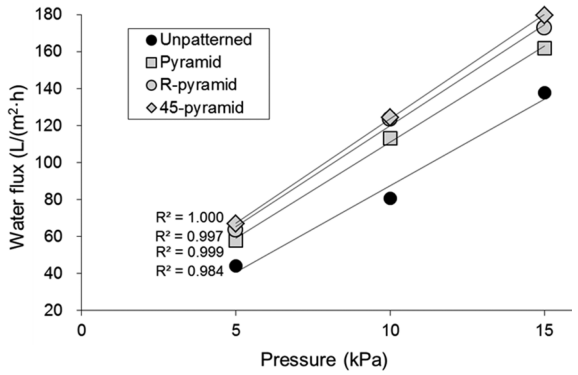

Figure 2. Apparent pure water flux of unpatterned and patterned membranes. The apparent pure water flux of the membranes was calculated using the apparent membrane surface area (4 cm^2), which is constant for all patterned membranes. The linearity in water flux as a function of pressure indicates that water permeability is almost constant in the pressure range. The averages and standard deviations for water permeability values are given in Table S1.

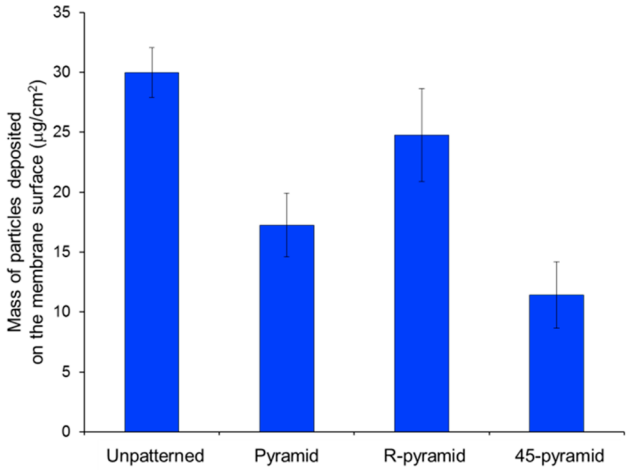

Figure 3. Particle deposition on the surface of unpatterned and patterned membranes (n = 3).

whereas the R-pyramid patterned membrane only slightly reduced the level of particle deposition compared with that of the unpatterned membrane.

Shear Stress on Unpatterned and Patterned Membrane Surfaces. The wall shear stresses of unpatterned and patterned membranes are presented in Figure 4. The red and blue colors of the vertical bar indicate relatively high and low shear stress values, respectively. On the unpatterned membrane surface, the shear stress was uniform (Figure 4a). On the other hand, the wall shear stress increased largely near the apexes of the pyramid and 45-pyramid patterns, as shown by the red color (Figure 4b,d). The strong shear stress induced by the patterns explains why pyramid and 45-pyramid patterns exhibited the lowest level of particle deposition, as shown in Figure 3. The maximal wall shear stress on each membrane surface is plotted in Figure 4e to provide a quantitative comparison between shear stresses of the patterned membranes. The values for the pyramid and 45-pyramid patterns were higher than those of the unpatterned and R-pyramid patterns, which explains the particle deposition results discussed above.

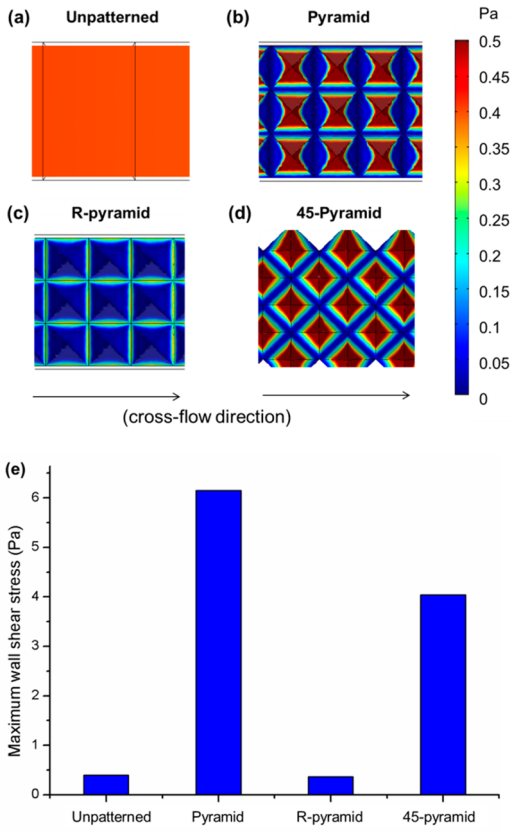

Figure 4. Shear stress distribution and maximal shear stress on the membrane surface. As shown on the scale bar of 0−0.5 Pa, the red and blue colors represent high and low shear stress values, respectively. A shear stress of >0.5 Pa is also colored red. (a) The unpatterned membrane surface induced uniform shear stress, whereas (b−d) patterned membranes showed different shear stress distributions depending on pattern shape. (e) Maximal shear stress on the membrane surface.

However, there were blue regions in correspondence of the valleys between pyramids (Figure 4b,d) where the shear stress was even lower than that of an unpatterned membrane. Particles have a strong tendency to collect in these areas, which weakens the antifouling properties of pyramid and 45-pyramid patterns.

Among the differences between the pyramid and 45-pyramid patterns, the relative ratio of red and blue (i.e., high- and low-shear, respectively) regions can be noted. For the pyramid pattern, the flow velocity near the sloped face perpendicular to the crossflow direction (left to right in Figure 4) is expected to be much lower than the slope face parallel to the crossflow. Thus, the face perpendicular to the flow direction showed more low-shear regions than the face parallel to the flow did (Figure 4b). However, in the case of the 45-pyramid pattern, where the patterns are rotated by 45°, the sloped faces were never perpendicular to the crossflow direction. As a result, the overall low-shear regions of the 45-pyramid pattern were smaller than those of the pyramid pattern (Figure 4d). Therefore, the level of particle deposition on the 45-pyramid pattern was lower than that on the pyramid pattern.

Meanwhile, as shown in Figure 4c, the R-pyramid pattern exhibited more low-shear regions than either the pyramid or the 45-pyramid pattern did. In this pattern, very narrow high-shear regions are present only on the top edges. The shear

DOI: 10.1021/acs.estlett.6b00468
Environ. Sci. Technol. Lett. XXXX, XXX, XXX−XXX

stress of the blue-colored, low-shear regions of the R-pyramid pattern was much lower than that of the unpatterned membrane, even though the maximal shear stresses of the R-pyramid-patterned and unpatterned membranes were similar, as shown in Figure 4e. This shear stress analysis indicates that the R-pyramid pattern should display the higher level of particle deposition and thus the worst antifouling properties. However, this conclusion is in contrast with the experimental results, showing that the R-pyramid pattern membrane exhibited a level of particle deposition lower than that of the unpatterned membrane as shown in Figure 3. This implies that the particle deposition cannot be fully explained in terms of only shear stress. This finding is understood by additionally analyzing flow regime characteristics near the surface in the following section.

Flow Regime near the Unpatterned and Patterned Membrane Surfaces. Streamlines at each membrane surface were obtained using the CFD method, which yielded flow direction and velocity distribution (Figure 5). Straight laminar flow was shown on the unpatterned membrane (Figure 5a), whereas patterned membranes displayed more complicated flow regimes (Figure 5b–d). In the case of the R-pyramid pattern, vortexes were formed at the pattern valleys (Figure 5c). The vortex streamlines were separated from bulk flow streamlines passing from left to right laterally. The vortex and flow separation were effective in preventing particles from moving toward the valleys and thus from depositing on the inside of the R-pyramid pattern, consistent with the results of our previous study.[12] Therefore, the R-pyramid pattern led to a level of particle deposition lower than that of the unpatterned membrane, despite its lower-shear regions.

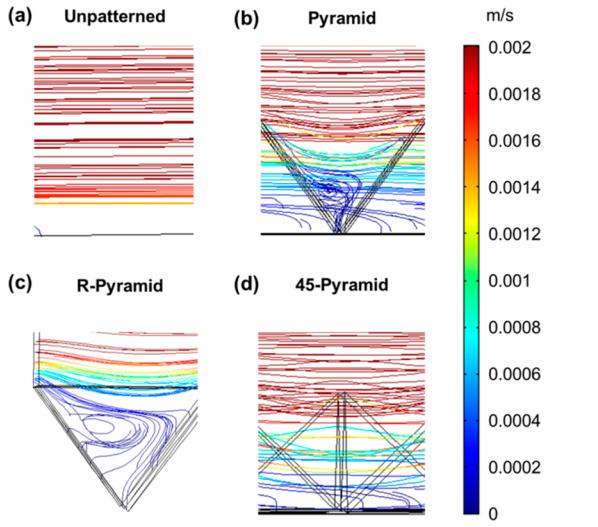

Figure 5. Streamlines near the surface of (a) unpatterned and (b–d) patterned membranes. The red and blue colors indicate high and low flow velocity values, respectively.

Figure 5b shows that there were also vortexes in the valley regions of the pyramid pattern, although the level of particle deposition on this membrane was greater than that measured on the 45-pyramid pattern, for which there were no vortexes, as shown in Figure 5d. We hypothesize that this result is due to the incomplete formation of these vortexes on the pyramid pattern. The valleys of the pyramid pattern are more exposed to the bulk flow than the valleys of the R-pyramid pattern are. Consequently, the vortexes on the pyramid pattern were smaller and incomplete compared with the R-pyramid pattern, as shown in Figure 5b. Additionally, many of the vortex streamlines of the pyramid pattern were directed toward the bottom of the end of the valley, which enhances particle deposition. This analysis could explain why the pyramid pattern showed a level of particle deposition, despite its vortex, higher than that of the 45-pyramid pattern.

Furthermore, the stream velocity at the pattern valleys was smaller on the pyramid pattern than on the 45-pyramid pattern, as depicted in panels b and d of Figure 5. Specifically, at the same height above the surface (around the center of the vortex in Figure 5b), the streamline color is blue in Figure 5b but yellow in Figure 5b. These results also explain the level of particle deposition observed on the pyramid pattern being higher than that on the 45-pyramid pattern.

The antifouling property of a patterned membrane is likely to vary as a function of pattern size, space between patterns, etc., for the same pattern shape, as shown in our previous study;[11] this was not investigated in this study to focus on the difference in pattern shape. Also, although a single-sized particle was used for the particle deposition tests in this study, the particle deposition on the membrane surface in crossflow filtration can differ according to the particle size and/or the relative size of the pattern and particle for a polydisperse particle solution.[13] These additional parameters affecting the antifouling property of patterns will be studied in the future.

In addition, it will be necessary to examine the feasibility of various patterned membranes in practical water and wastewater processes by applying the patterned membranes to filtration systems employing real or synthetic raw water sources, as reported previously.[14]

■ ASSOCIATED CONTENT

Supporting Information

The Supporting Information is available free of charge on the ACS Publications website at DOI: 10.1021/acs.estlett.6b00468.

Additional details about materials and methods and supplementary tables and figures mentioned in the text (PDF)

■ AUTHOR INFORMATION

Corresponding Authors

*Phone: +82-33-760-2890. E-mail: pkpark@yonsei.ac.kr.
*Phone: +82-2-880-7075. Fax: +82-2-874-0896. E-mail: leech@snu.ac.kr.

ORCID

Pyung-Kyu Park: 0000-0003-3715-1913

Notes

The authors declare no competing financial interest.

■ ACKNOWLEDGMENTS

This work was supported by a National Research Foundation of Korea grant funded by the Korean Government (MEST) (NRF-2010-C1AAA001-0029061) and also by the Korea Ministry of Environment (MOE) as “Knowledge-based environmental service Human resource development Project”.

■ REFERENCES

(1) Bacchin, P.; Aimar, P.; Sanchez, V. Influence of surface interaction on transfer during colloid ultrafiltration. *J. Membr. Sci.* **1996**, *115*, 49–63.

DOI: 10.1021/acs.estlett.6b00468
Environ. Sci. Technol. Lett. XXXX, XXX, XXX–XXX

(2) Hong, S.; Faibish, R. S.; Elimelech, M. Kinetics of permeate flux decline in crossflow membrane filtration of colloidal suspensions. *J. Colloid Interface Sci.* **1997**, *196*, 267−277.
(3) Altmann, J.; Ripperger, S. Particle deposition and layer formation at the crossflow microfiltration. *J. Membr. Sci.* **1997**, *124*, 119−128.
(4) Li, H.; Fane, A. G.; Coster, H. G. L.; Vigneswaran, S. Direct observation of particle deposition on the membrane surface during crossflow microfiltration. *J. Membr. Sci.* **1998**, *149*, 83−97.
(5) Culfaz, P. Z.; Buetehorn, S.; Utiu, L.; Kueppers, M.; Blue mich, B.; Melin, T.; Wessling, M.; Lammertink, R. G. H. Fouling behavior of microstructured hollow fiber membranes in dead-end filtrations: critical flux determination and NMR imaging of particle deposition. *Langmuir* **2011**, *27* (5), 1643−1652.
(6) Culfaz, P. Z.; Haddad, M.; Wessling, M.; Lammertink, R. G. H. Fouling behavior of microstuctured hollow fibers in cross-flow filtrations: Critical flux determination and direct visual observation of particle deposition. *J. Membr. Sci.* **2011**, *372* (1−2), 210−218.
(7) Culfaz, P. Z.; Rolevink, E.; van Rijn, C.; Lammertink, R. G. H.; Wessling, M. Microstructured hollow fibers for ultrafiltration. *J. Membr. Sci.* **2010**, *347* (1−2), 32−41.
(8) Culfaz, P. Z.; Wessling, M.; Lammertink, R. G. H. Hollow fiber ultrafiltration membranes with microstructured inner skin. *J. Membr. Sci.* **2011**, *369* (1−2), 221−227.
(9) Culfaz, P. Z.; Wessling, M.; Lammertink, R. G. H. Fouling behavior of microstructured hollow fiber membranes in submerged and aerated filtrations. *Water Res.* **2011**, *45* (4), 1865−1871.
(10) Won, Y. J.; Lee, J.; Choi, D. C.; Chae, H. R.; Kim, I.; Lee, C. H.; Kim, I. C. Preparation and application of patterned membranes for wastewater treatment. *Environ. Sci. Technol.* **2012**, *46* (20), 11021−11027.
(11) Won, Y. J.; Jung, S. Y.; Jang, J. H.; Lee, J. W.; Chae, H. R.; Choi, D. C.; Ahn, K. H.; Lee, C. H.; Park, P. K. Correlation of membrane fouling with topography of patterned membranes for water treatment. *J. Membr. Sci.* **2016**, *498*, 14−19.
(12) Choi, D. C.; Jung, S. Y.; Won, Y. J.; Jang, J. H.; Lee, J. W.; Chae, H. R.; Ahn, K. H.; Lee, S.; Park, P. K.; Lee, C. H. Three-dimensional hydraulic modeling of particle deposition on the patterned isopore membrane in crossflow microfiltration. *J. Membr. Sci.* **2015**, *492*, 156−163.
(13) Jang, J. H.; Lee, J.; Jung, S. Y.; Choi, D. C.; Won, Y. J.; Ahn, K. H.; Park, P. K.; Lee, C. H. Correlation between particle deposition and the size ratio of particles to patterns in nano- and micro-patterned membrane filtration systems. *Sep. Purif. Technol.* **2015**, *156*, 608−616.
(14) Kim, I.; Choi, D. C.; Lee, J.; Chae, H. R.; Jang, J. H.; Lee, C. H.; Park, P. K.; Won, Y. J. Preparation and application of patterned hollow-fiber membranes to membrane bioreactor for wastewater treatment. *J. Membr. Sci.* **2015**, *490*, 190−196.

DOI: 10.1021/acs.estlett.6b00468
Environ. Sci. Technol. Lett. XXXX, XXX, XXX−XXX